Side-chain polarity modulates the intrinsic conformational landscape of model dipeptides

Debayan Chakraborty,[*,†] Atreyee Banerjee,[‡,¶] and David J. Wales[*,‡]

†*Department of Chemistry, The University of Texas at Austin, 24th Street Stop A5300, Austin TX 78712, USA.*

‡*Yusuf Hamied Department of Chemistry, University of Cambridge, Lensfield Road, Cambridge CB2 1EW, UK.*

¶*Max Planck Institute for Polymer Research, 55128 Mainz, Germany*

E-mail: debayan.chakraborty@utexas.edu; dw34@cam.ac.uk

Abstract

The intrinsic conformational preferences of small peptides may provide additional insight into the thermodynamics and kinetics of protein folding. In this study, we explore the underlying energy landscapes of two model peptides, namely, Ac-Ala-NH_2, and Ac-Ser-NH_2, using geometry optimization based tools developed within the context of energy landscape theory. We analyse how side-chain polarity not only influences the structural preferences of the dipeptides, but also other emergent properties of the landscape, including heat capacity profiles, and kinetics of conformational rearrangements. The contrasting topographies of the free energy landscape agree with recent results from Fourier transform microwave spectroscopy experiments, where Ac-Ala-NH_2 was found to exist as a mixture of two conformers, while Ac-Ser-NH_2 remained structurally locked, despite exhibiting an apparently rich conformational landscape.

Introduction

Despite decades of research, the protein folding problem[1,2] continues to attract great interest. The major advances in specialized hardware,[3] as well as deep-learning techniques,[4] now make it possible to study proteins of varying complexities and topologies using computer simulations, and provide the much-needed atomistic insight into biophysical experiments.[5,6] There are essentially two facets to the folding problem: the first one is related to structure prediction and thermodynamics, and includes the characterization of three-dimensional structures, which dominate the equilibrium population. These structures are usually associated with specific biological functions within the cellular machinery. The second problem concerns folding mechanisms and kinetics, which describe how a protein molecule relaxes to its functional three-dimensional conformation starting from a relatively unstructured configuration by navigating along well-defined folding routes on the underlying energy landscape.[7,8] In addition to the intramolecular energetics, as dictated by the interactions among the constituent amino acids, intermolecular interactions with the surrounding environment also have a pro-

nounced effect on the folding thermodynamics and kinetics. As shown in previous studies, solvent polarity, pH,[9–11] as well as the presence of crowding agents,[12,13] and denaturants[14,15] significantly reshape the folding landscape, thereby altering its emergent properties.

The synergy between intra- and intermolecular interactions exacerbates the complexity of the folding process, making it rather difficult to formulate general principles that would advance our understanding of the structure-function paradigm. A first step in this direction is to explore the intrinsic conformational preferences of protein sequences, particularly, small peptides and peptidomimetics, in the absence of interactions with the surroundings. Experiments carried out in the gas phase provide the ideal medium for such studies, and help to discern the interplay of intramolecular interactions that lend stability to the protein molecule, and dictate its three-dimensional structure.[16] While double resonance experiments have long been exploited to investigate the structural features of small peptides,[17–23] microwave spectroscopy has recently emerged as a potential alternative. In recent studies,[24–34] Alonso and coworkers have determined the structures of the dominant conformers for a range of capped dipeptides, using a combination of the laser ablation technique and Fourier transform microwave spectroscopy. The authors conclusively show that the polarity of the side chain plays a key role in dictating the conformational equilibrium of the dipeptides, through the locking of specific configurations.[29,30] In addition to gas-phase experiments, a number of theoretical studies have characterized the potential energy landscape (PEL) for different dipeptides, using molecular mechanics as well as *ab initio* methods. Tobias and Brooks used the CHARMM force field to study the conformational equilibria of the alanine dipeptide both in the gas phase, and in water, and observed a pronounced solvent effect.[35] In another study, Vondrášek and coworkers[36] used metadynamics simulations to explore the free energy landscape of the alanine dipeptide in vacuum, as well as in water, for three different parameterizations of the AMBER force field. The populations of the different secondary structure elements predicted by the authors were found to be in reasonable agreement with those estimated using vibrational spectroscopy.[37] Systematic benchmarking on model pep-

tides carried out by Jensen and coworkers[38] revealed that the commonly used biomolecular force fields based on fixed charged models could not reproduce the reference data from high-level quantum mechanical calculations, and multiple moments and polarizability needed to be accounted for to obtain any reasonable agreement.

Using Hartree-Fock (HF) and Moller-Plesset (MP) perturbation theory, Pople and coworkers explored the PELs for blocked alanine and glycine dipeptides,[39] and showed that the steric effect induced by the methyl side-chain of the alanine dipeptide had a profound effect on its conformational preferences. In a later study, Gould *et al.* corroborated these findings, although different capping groups and basis sets were used to model the dipeptides.[40] Subsequently, several benchmark studies[41–44] on the alanine dipeptide comparing different levels of theory have emerged. In a recent work, Fedorov and coworkers[45] exploited a hybrid approach combining systematic scanning of the PEL, and *ab initio* molecular dynamics to study the alanine dipeptide system. Interestingly, the authors identified several new minima, not characterized in earlier work, suggesting that the PELs of simple dipeptides in the gas phase, often used as a proxy to understand the principles underlying protein folding, can exhibit unexpected features. While most of these studies have primarily focused on elucidating the thermodynamic features of the underlying landscape, Salahub and coworkers estimated the characteristic timescale of interconversion between the two prominent conformers of alanine dipeptide, namely C_7^{eq} and C_5, employing *ab initio* molecular dynamics within the framework of Kohn-Sham density functional theory.[46] They noted that the transitions between the two conformers occur on the picosecond timescale, in apparent disagreement with classical molecular dynamics simulations, in which no interconversion events were observed even after nanoseconds.

In this work, we systematically explore the PELs for two model dipeptides, namely N-acetyl-alaninamide (Ac-Ala-NH_2), and N-acetyl-serinamide (Ac-Ser-NH_2), in the gas phase using geometry optimization based computational tools developed within the framework of energy landscape theory.[8,47,48] We use basin-hopping (BH) global optimization[49,50] in con-

junction with gas-phase molecular dynamics to identify low-lying minima on the PEL, and Discrete Path Sampling (DPS)[51,52] to locate the intervening transition states. The rearrangement pathways between the distinct peptide conformations are described geometrically in terms of interconnected minimum-transition state-minimum triples on the PEL, rendering an *a priori* choice of reaction coordinates unnecessary. Our approach is largely complementary to 'rare event' sampling schemes based on explicit dynamics,[53–60] which are routinely used to study folding surrogates, such as dipeptides, for both benchmarking and force field development.

We find that for both Ac-Ala-NH_2 and Ac-Ser-NH_2, the C_7^{eq} conformer corresponds to the free energy global minimum at 298 K, in agreement with previous experimental[29,33,61] and theoretical studies.[39,40,43] As anticipated by Alonso and coworkers,[29,33] the presence of a polar side-chain in Ac-Ser-NH_2 makes its underlying energy landscape somewhat more complex compared to Ac-Ala-NH_2, and leads to distinct thermodynamic as well as kinetic features. The free energy gap, ΔF at 298 K between the C_7^{eq} and C_5 conformers of Ac-Ala-NH_2 is small, (around 0.03 k_BT), explaining their coexistence, and simultaneous detection in the supersonic expansion based on their rotational signatures.[29] On the other hand, $\Delta F \approx 2k_BT$ for Ac-Ser-NH_2, and the C_7^{eq} conformer dominates the equilibrium population.

Computational Methodology

The initial structures of the capped dipeptides, Ac-Ala-NH_2 and Ac-Ser-NH_2, were constructed using the *tleap* module available within the AMBER14 code.[62] The dipeptides were modeled using the AMBERff14SB force field.[63] A preliminary exploration of the conformational space was first carried out *in vacuo* using short molecular dynamics (MD) simulations of around 2 microseconds. The temperature was maintained at 298 K using a Langevin thermostat,[64] employing a collision frequency of 1.0 ps^{-1}. These simulations were carried out using the AMBER14 code.[62] Snapshots from the MD trajectories were periodically quenched

to build an initial database of minima.

We then employed basin-hopping (BH) global optimization,[49,50] as implemented within the interfaced version of the GMIN code[65] with the AMBER9[66] package, to locate low-lying minima that could have been missed by finite temperature MD simulations. As shown in previous work,[49,67–69] BH has been successful in locating the putative global minima for a wide range of atomic and molecular systems characterized by landscapes with broken ergodicity. The key idea in BH is to transform the multidimensional PEL into a set of interpenetrating catchment basins, comprising the local minima. The transformation does not change the global minimum or the relative ordering of the local minima. However, the downhill barriers between the local minima in the different basins are removed.[47] The basin transformation is coupled with steps between local minima to explore the configuration space. For each dipeptide, one hundred separate BH runs with different random number seeds, were carried out. Group rotation moves (rigid body rotation of a group of atoms about a predefined axis), in conjunction with random Cartesian displacements, were employed to perturb the coordinates of the current local minimum. Local minimization was carried out for each BH step using a modified version of the L-BFGS algorithm.[70] The new minimum, thus generated, was accepted/rejected based on the Metropolis criterion.

Discrete path sampling (DPS)[51,52] was employed for further exploration of the PEL. The DPS procedure has been previously used to construct databases of stationary points (kinetic transition network) for a wide range of systems,[71–77] and provide insight into conformational transitions spanning a hierarchy of timescales. Within the DPS framework, the connectivity between different regions of the PES is described in terms of discrete paths, consisting of an interconnected sequence of local minima, and intervening transition states. In accordance with the Murrell-Laidler definition,[78] any stationary point with a single imaginary frequency (with the associated eigenvector corresponding to a reaction coordinate) is characterized as a transition state. The adjoining minima are connected to the transition state via approximate steepest-descent paths directed parallel and antiparallel to the eigenvector corresponding to

the unique negative Hessian eigenvalue.

DPS runs were carried out to connect the different local minima identified from BH in a pairwise fashion. Initial guesses for the intervening transition states were obtained using the doubly-nudged[79] elastic band[80,81] (DNEB) method. The hybrid eigenvector-following scheme[82] was then used to accurately converge the candidate transition state structures obtained from DNEB, until the root-mean-square (RMS) gradient fell below 10^{-6} kcal/mol Å^{-1}. All the local minimizations and transition state searches were carried out using the OPTIM code[83] interfaced with AMBER9.[66] As the initial discrete paths found between the different pairs of minima are unlikely to be kinetically relevant, they were further refined using various sampling schemes available within the PATHSAMPLE code.[84] Specifically, the SHORTCUT BARRIER and SHORTCUT schemes, described in previous work,[85] were used to locate pathways characterized by lower potential energy barriers, and shorter path lengths, respectively. However, these pathway refinement schemes often lead to undersampling of some regions of the PEL, manifested in the form of artificial frustration. The UNTRAP scheme,[85] as implemented within the PATHSAMPLE code, was used to remove this artificial frustration by systematically reconnecting selected local minima to the global minimum. This criterion for selecting minima for the connection-making attempts is based on the ratio of the potential energy barrier to the potential energy difference relative to the global minimum. The databases were expanded by sequential applications of these three refinement schemes, until no further stationary points were located. The rearrangement pathways between different dipeptide conformers were extracted from the transition network using Dijkstra's shortest path algorithm[86] with appropriate edge-weights.

The harmonic superposition approximation (HSA)[87,88] was used to estimate the free energies from the stationary point databases obtained from DPS. Within the HSA, the overall canonical partition function is written as a sum of contributions from the catchment basin of each local minimum:[47]

$$Z(T) = \sum_{i=1}^{M} Z_i(T), \tag{1}$$

In Eq. (1), M is the total number of minima in the stationary point database. The canonical partition function $Z_i(T)$ for local minimum i is expressed as:[47]

$$Z_i(T) = \frac{n_i \exp(-V_i/k_BT)}{(h\bar{\nu}_i/k_BT)^\kappa}. \tag{2}$$

Here, V_i denotes the potential energy of local minimum i, n_i is the number of distinct permutation-inversion isomers of i, and $\bar{\nu}_i$ is the geometric mean of the normal mode frequencies associated with minimum i, and κ is the number of vibrational degrees of freedom.

The local free energy $F_i(T)$, and the corresponding equilibrium occupation probability $p_i^{eq}(T)$, of minimum i are:[47]

$$F_i(T) = -k_BT \ln Z_i(T), \tag{3}$$

and

$$p_i^{eq}(T) = \frac{Z_i(T)}{Z(T)}. \tag{4}$$

The partition functions, and the free energies corresponding to the transition states in the stationary point database, have the same forms as those in Eq. (1) and (2), except that the normal mode corresponding to the imaginary frequency is excluded from the geometric mean. The heat capacity, C_v is defined in terms of the partition function, $Z(T)$, using standard relations from equilibrium thermodynamics:

$$C_v = \left(\frac{\partial V(T)}{\partial T}\right)_{N,V}, \tag{5}$$

In Eq. (5), $V(T)$ is the internal energy. Using Eq. (1), the C_v corresponding to the superposition partition function can be expressed as:

$$C_v = \kappa k_B - \frac{z_1(T)^2}{k_BT^2 z_0(T)^2} + -\frac{z_2(T)^2}{k_BT^2 z_0(T)} \tag{6}$$

where

$$z_r(T) = \sum_i n_i (V_i)^r \left(\frac{k_B T}{h\bar{\nu}_i} \right)^{\kappa} \exp(-V_i/k_B T) \tag{7}$$

Harmonic transition state theory (TST) is used to compute the minimum-to-minimum rate constants:

$$k_i^{\dagger}(T) = \frac{kT}{h} \frac{Z^{\dagger}(T)}{Z_i(T)} e^{-\beta \Delta V} \tag{8}$$

In Eq. (8), $Z^{\dagger}(T)$ denotes the partition function of the transition state; $Z_i(T)$ is the partition function of minimum i; ΔV is the potential energy difference between the transition state and minimum i. For an elementary transition from minimum i to minimum j, the total rate constant $k_{ji}(T)$ is obtained by summing the the $k_i^{\dagger}(T)$ values for all transition states that connect the two minima. The overall rate constants between a reactant (A) and product (B) states can be expressed in terms of these minimum-to-minimum rate constants, k_{ji}, in conjunction with a Markovian assumption for the dynamics between adjacent minima. When the steady-state approximation is relaxed, we obtain the phenomenological rate constants or equivalently the mean first passage times between A and B, which describe the global dynamics. The new graph transformation (NGT) method[89,90] is used to extract these global dynamical observables. For further details regarding the formalism, we refer the readers to the original references.[51,52,90]

The potential and free energy landscapes of the dipeptides were visualized using disconnectivity graphs.[91,92] This representation of the landscape is simple, yet powerful, and preserves the barriers between different local minima, in contrast to low-dimensional projection-based approaches that may introduce artefacts.[93,94]

To obtain refined estimates of relative energies and barriers, the local minima corresponding to different dipeptide conformations, as well transition states connecting them, were further reoptimized in the gas phase at the MP2 level of theory using 6-311++G(d,p) basis sets. Previous work has shown that this level of theory is appropriate for describing the conformational preferences of small peptides.[24,33,95] The geometry optimizations were

carried out using the GAUSSIAN09 package[96] interfaced to the OPTIM code.[83]

Results and Discussion

Initial exploration of the conformational space: The two dipeptides can access different conformations (Figure 1 and Table S1) on the timescale of the MD simulations. The conformational space can be segregated on the basis of Ramachandran angles (ϕ, ψ), following the convention described in the study of Perez and coworkers.[97] We find snapshots corresponding to all the nine conformer families, for both the dipeptides, which suggests that our initial sampling based on MD is adequate, even if not exhaustive. As observed in earlier work,[97] some of the conformers are not true geometric minima on the gas phase PEL, and relax to other geometries upon minimization. For Ac-Ala-NH_2, there are only four potential energy minima, corresponding to the C_7^{eq}, C_5, C_7^{ax}, and the P_{II} conformer families. Although a large number of β_2 conformers are sampled along the MD trajectory, a majority of them relax either to the C_5 or the C_7^{eq} form, and a minor population relaxes to the P_{II} geometry upon quenching. Most structures belonging to the P_{II} conformational cluster switch to either the C_7^{eq} or the C_5 form after local minimization, and only a few of them stay in the P_{II} basin. The MD simulation also samples a significant number of α_R conformations. However, all of them relax to the C_7^{eq} minimum after geometry optimization (Supporting Information, Figure S1). The α' conformer, which is adjacent to α_R in the Ramachandran plot, also relaxes to the C_7^{eq} minimum upon quenching. On the other hand, all the α_L and α_D conformations relax to the C_7^{ax} minimum.

For Ac-Ser-NH_2, we find that, in addition to C_7^{eq}, C_5, C_7^{ax}, and P_{II}, the β_2 and α', and α_D conformers are also associated with basins of attraction on the PEL (Figure 1). However, a major population of β_2 conformations still relax to either the C_7^{eq} or C_5 geometry on local minimization. A majority of the P_{II} structures also switch to C_7^{eq} after quenching. As for Ac-Ala-NH_2, all of the α_R conformations relax to C_7^{eq}, and α_L conformations relax to the

C_7^{ax} form after geometry optimization. Only one out of all the sampled α' conformations quenches to the α' basin, and the rest relax to the C_7^{eq} geometry upon local minimization. Of the two α_D structures of Ac-Ser-NH_2 that are sampled along the MD trajectory, one remains in α_D geometry upon quenching, while the other switches to the C_7^{ax} form. For both Ac-Ala-NH_2 and Ac-Ser-NH_2, only two snapshots out of 1×10^5 adopt the α_D conformation. Our results suggest that for both the dipeptides *in vacuo*, the α_D conformer is a high free energy minimum (if a true minimum at all), in accord with a number of previous studies employing different molecular mechanics force fields.[53,54,98] In fact, systematic benchmarking of different *ab initio* methods[40,41,45,99] shows that the α_D conformer is not a minimum on most potential energy surfaces.

To ensure that our initial sampling based on microsecond MD did not miss any relevant low-lying minimum on the PEL, we initiated BH simulations from random starting configurations of the two dipeptides. BH did not locate any new potential energy minimum, other than those already identified from the MD trajectories, suggesting that a proper exploration of the low-lying region of the underlying landscape has been achieved. The distinct low-energy conformers of Ac-Ala-NH_2 and Ac-Ser-NH_2 are shown in Figure 1. For both the dipeptides, the folded C_7^{eq} conformer corresponds to the potential energy global minimum. As pointed out in earlier work,[33] the stabilization of the C_7^{eq} conformer can be attributed to the formation of a seven-membered ring, in which an intramolecular hydrogen-bond is formed between the acetyl carbonyl oxygen, and one of the terminal amide hydrogens. The fully extended C_5 conformer is the second-lowest minimum for Ac-Ala-NH_2, and is destabilized with respect to the C_7^{eq} conformer by only ≈ 0.3 kcal/mol. This value is somewhat lower than that predicted by different *ab initio* methods,[33,41,99,100] and could be due to the deficiencies associated with the AMBER force field.[36,101,102] The P_{II} minimum does not have the hydrogen-bond between the carbonyl and the amide moieties, and is destabilized by around 1.1 kcal/mol relative to the C_7^{eq} conformer. The C_7^{ax} conformer also exhibits a seven-membered ring, much like C_7^{eq}. However, it is destabilized by around 1.6 kcal/mol because

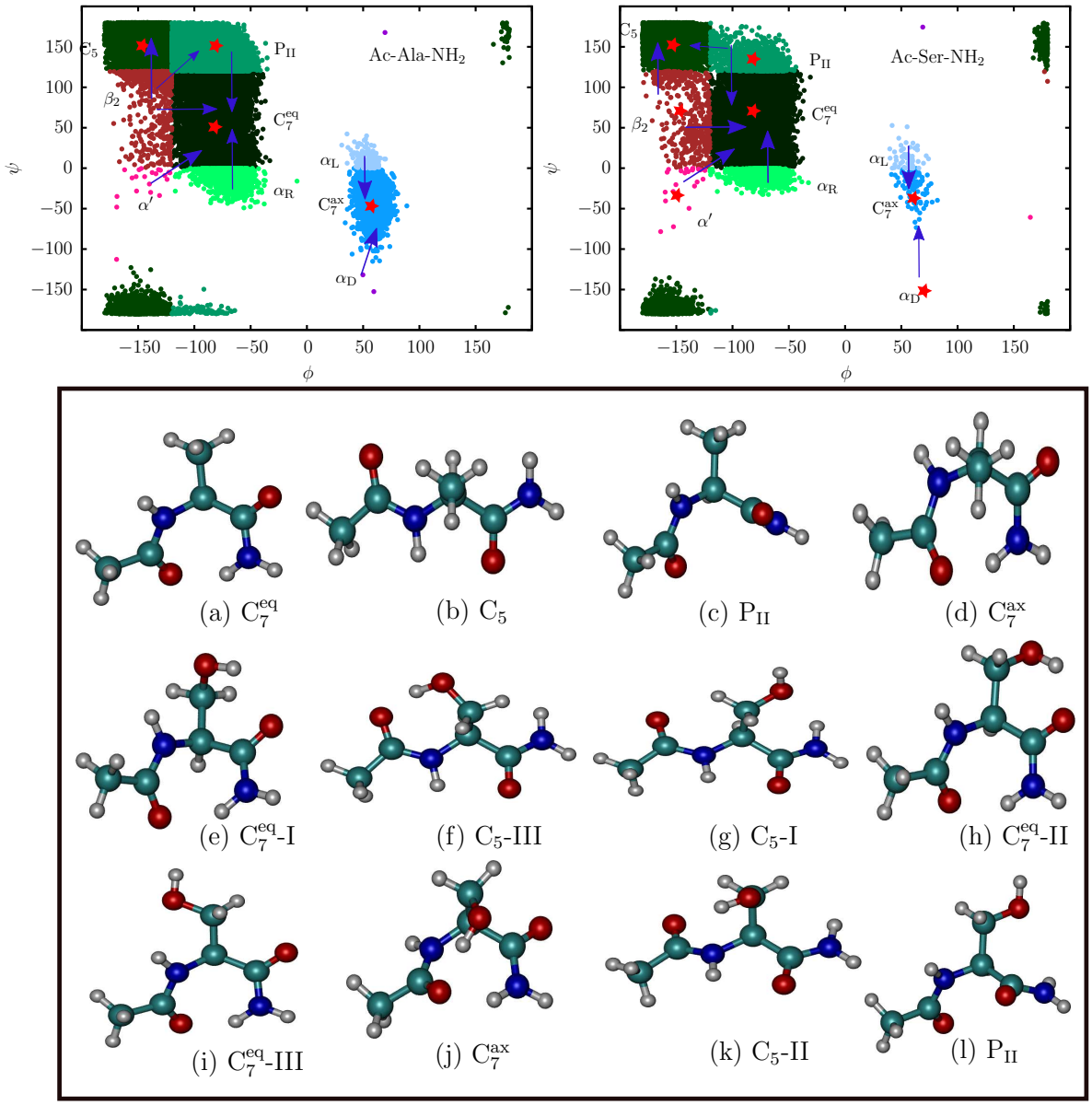

Figure 1. Top panel: The different conformations sampled along the gas-phase MD trajectories are shown on the Ramachandran map (left: Ac-Ala-NH_2; right: Ac-Ser-NH_2). The red stars denote the different potential energy basins that are identified after local minimization of snapshots from the MD trajectories at regular intervals. The blue arrows indicate the specific basins that the different conformations fall into after local minimization. The thickness of the arrows is approximately proportional to the probability of visiting a particular local minimum. The conformers are labeled according to the Ramachandran angles (ϕ, ψ), following the convention described in the study of Perez and coworkers.[97] Bottom panel: Distinct low-energy conformers of the dipeptides. (a)-(d) denote the different conformers of Ac-Ala-NH_2. (e)-(l) denote the different conformers of Ac-Ser-NH_2. The β_2, α', and α_D conformers of Ac-Ser-NH_2, which are destabilized relative to the global minimum by more than 6 kcal/mol are not shown.

of the axial orientation of the methyl group that results in a steric repulsion between the C_β atom and the seven-membered ring.[45] The relative ordering of the different conformers are in agreement with previous studies on different alanine dipeptide analogues.[41,45,99,103–105]

For Ac-Ser-NH_2, three distinct low-energy C_7^{eq} conformers are identified, which differ primarily in the orientation of the side-chain. Two of these conformers (C_7^{eq}-I and C_7^{eq}-II) were reported before by Alonso and coworkers.[29] In terms of relative potential energies, C_7^{eq}-I $<$ C_7^{eq}-II $<$ C_7^{eq}-III. This order could be rationalized on the basis of the hydrogen-bonding interactions formed by the polar side-chain of Ser in the different conformations (Supporting Information, Figure S2). In C_7^{eq}-I, the side-chain is oriented equatorially, and it participates in two hydrogen-bonding interactions with the neighbouring -N–H and -C=O and groups. On the other hand, the side-chain in the C_7^{eq}-II forms a single hydrogen-bond with the -C=O group. The side-chain in C_7^{eq}-III only forms a weak hydrogen-bond with the -N–H group, and is destabilized by around 3.0 kcal/mol relative to the C_7^{eq}-I conformer.

In their study, Alonso and coworkers[29] also characterized three distinct C_5 conformers through systematic scanning of the conformational space using semi-empirical methods. These structures exhibit different interaction patterns involving the the side-chain hydroxyl group (Figure 1). The local minimization of MD snapshots, as well as BH simulations identify all these three C_5 conformers as low-energy minima of the landscape, lying within 4.3 kcal/mol of the potential energy global minimum (the C_7^{eq}-I conformer). In fact, the C_5-III and C_5-I conformers are lower in potential energy compared to the other two C_7^{eq} structures. These enhanced stabilities can also be explained in terms of the hydrogen-bonding networks formed by the polar side-chain in the two conformers (Supporting Information, Figure S2). In both structures, a six-membered ring is formed by the interaction between the side-chain hydroxyl group, and the acetyl carbonyl oxygen (C_5-III conformer), or one of the terminal amino hydrogens (C_5-I conformer). No such stabilization is immediately apparent for the C_5-II conformer, where the side-chain assumes an axial orientation. The C_7^{ax}, and the P_{II} conformers are higher in potential energy by $\approx$ 2.8 kcal/mol, and 5.3 kcal/mol, respectively,

relative to the C_7^{eq}-I structure. The pronounced destabilization of the P_{II} conformer relative to its alanine counterpart, can be attributed to the loss of all side-chain–backbone hydrogen-bonding interactions within this structure (Supporting Information, Figure S2).

Overall, a combination of MD and BH simulations reveal that the presence of a polar side-chain in Ac-Ser-NH_2 significantly alters the emergent features of the PEL. It not only produces new potential energy minima, corresponding to additional conformers (β_2, α', and α_D), but also increases the energy gap relative to the global minimum. In the following sections, we analyze the topological features of the free energy landscapes, as well as their emergent features, including heat capacity profiles, and rearrangement pathways among the different dipeptide conformers.

Different topographies of the energy landscapes: The potential energy minima sampled from MD and BH simulations form the initial database of stationary points. The intervening transition states between each pair of minima were identified using DPS simulations,[51,52] and the stationary point databases were expanded using the different refinement schemes,[85] until no new minima or transition states were found. The converged transition network for the Ac-Ala-NH_2 dipeptide consists of 13 minima, of which the lowest six were already identified using MD and BH simulations. The other seven minima with a *cis* peptide bond are located in the high energy region of the landscape. In addition, the network includes 102 transition states. There are 101 minima (with 57 of them exhibiting a *cis* peptide bond) and 850 transition states in the transition network for Ac-Ser-NH_2.

The free energy landscapes computed at 298 K for the Ac-Ala-NH_2 and Ac-Ser-NH_2 dipeptides are depicted in the form of disconnectivity graphs in Figures 2 and 3, respectively. The corresponding potential energy disconnectivity graphs are included in the Supporting Information (Figures S3 and S4). The branches of the graphs are colored according to the value of the ω torsion angle, which determines whether the peptide bond assumes the *cis* or the *trans* orientation. As expected, for both the dipeptides, the biologically relevant *trans* minima occupy the low-lying regions of the energy landscape. Overall, the topographies of

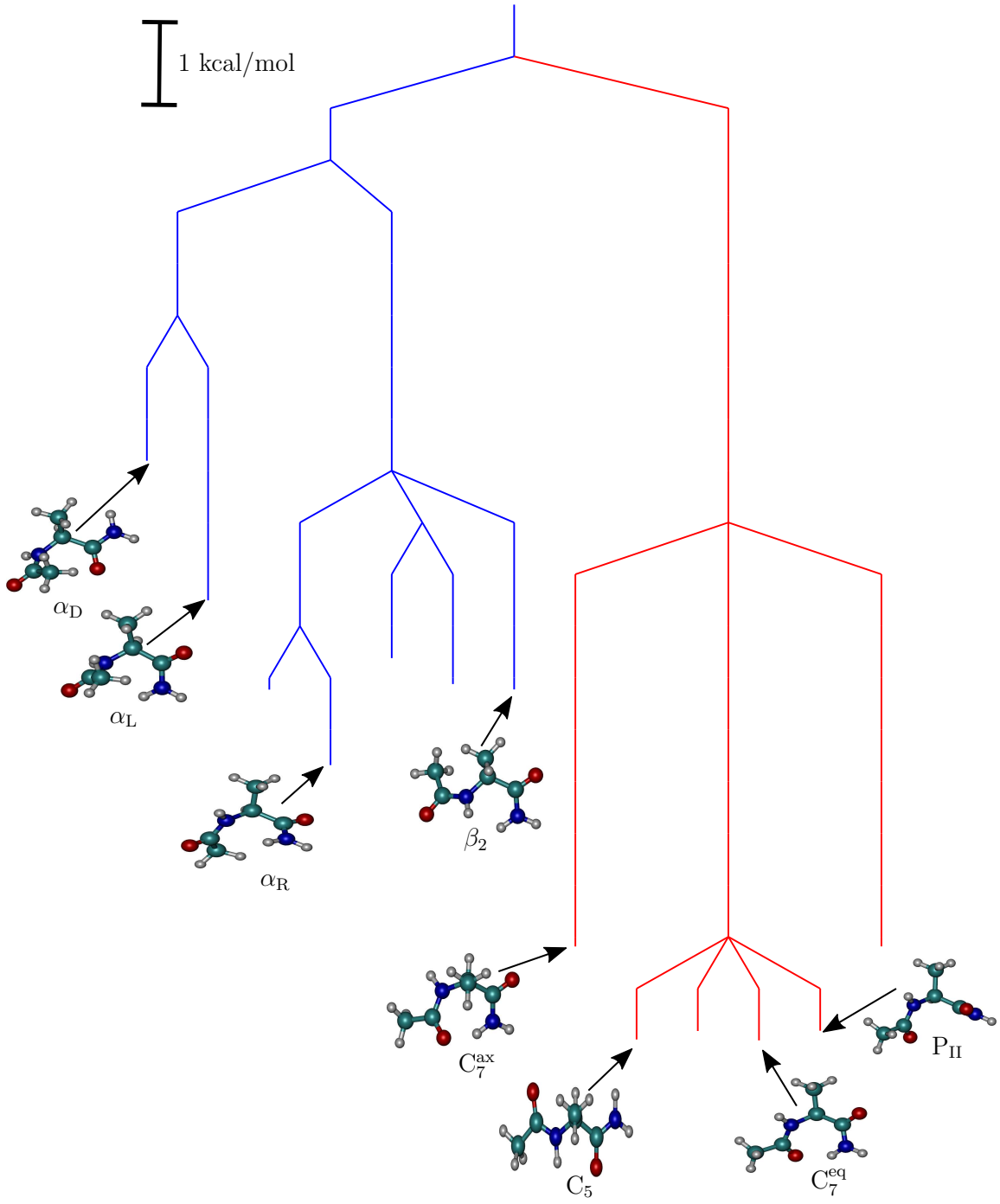

Figure 2. The free energy landscape for Ac-Ala-NH_2 computed at 298 K. The branches of the disconnectivity graph are colored according to the configuration that the peptide bond adopts about the ω torsion angle. Red branches lead to minima with *trans* peptide bonds, whereas blue branches lead to minima having *cis* peptide bonds. Snapshots corresponding to the distinct dipeptide conformers are shown superimposed on the graph.

both FELs seem consistent with earlier IR spectra for dipeptides recorded in an argon matrix,[106] as well as more recent rotational spectroscopy data from Alonso and coworkers.[29,33] The free energy barrier between the *cis* and *trans* funnels is approximately 13 kcal/mol, in good agreement with previous estimates.[107] Therefore, at physiological conditions, the *cis* configurations will not contribute significantly to the global thermodynamics, and peptide bond isomerizations will only occur at elevated temperatures.[107,108]

At 298 K, the free energy minima corresponding to the C_7^{eq} and C_5 conformers of Ac-Ala-NH_2 are nearly degenerate, with a free energy difference of only around 0.02 kcal/mol. The P_{II} conformer is also stabilized further due to entropic contributions. The C_7^{ax} conformer is destabilized relative to the C_7 conformer by ≈ 1.8 kcal/mol, and is separated from it by a free energy barrier of ≈ 7.3 kcal/mol. Our estimated values are in agreement with those previously reported in earlier studies based on different force fields and sampling techniques.[56,57,59] We find that the *cis* funnel is not a mirror image of the *trans* funnel, neither in terms of topography, nor in the organization of different minima. The stability of the conformers within each funnel is dictated by the sterically allowed intramolecular interactions that can be formed. The overall structure of the landscape within the *cis* and *trans* funnels is also dictated by the functional form of the torsion potential within the AMBER force field, which by construction is biased towards the *trans* configuration for all non-proline amino-acids. There is some evidence to suggest that a recalibration of the torsion potential could shift the conformational equilibria within the *cis* and *trans* funnels.[109] Within the *cis* funnel, we do not find any low-lying C_7^{eq} structure, and the α_R conformer corresponds to the lowest free energy minimum, followed by the β_2, α_L and α_D conformers. Interestingly, none of the *trans* counterparts of the low-lying *cis* conformers, correspond to minima on the FEL. A similar asymmetry in the organization of the conformational landscape has also been observed for peptoids,[110] as well as model dipeptides.[45]

The C_7^{eq}-I conformer is the free energy global minimum for Ac-Ser-NH_2, with the other C_7^{eq} and C_5 conformers occupying the low-energy regions of the FEL. Due to entropic stabi-

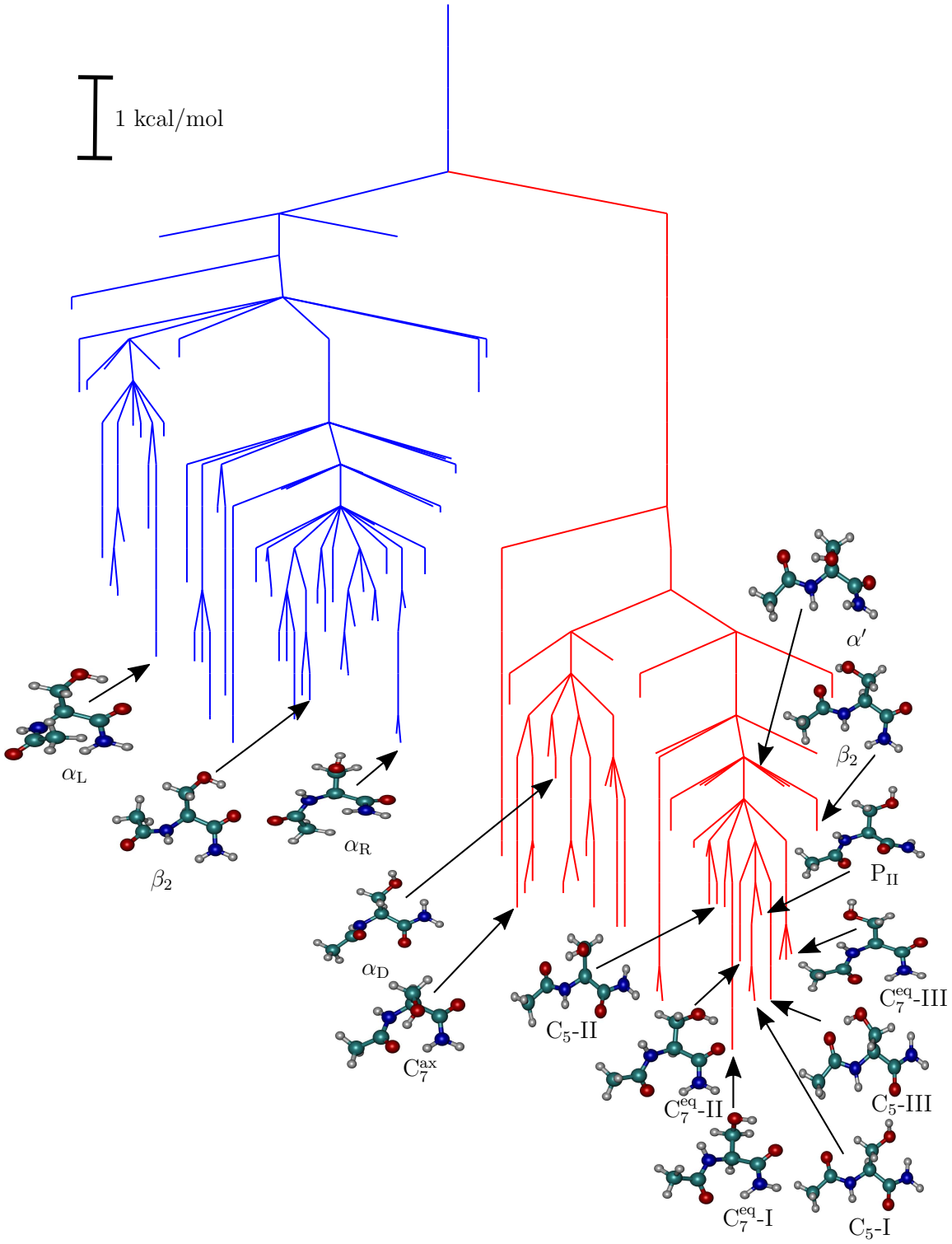

Figure 3. The free energy landscape of Ac-Ser-NH_2 computed at 298 K. The coloring scheme is the same as in Figure 2. Some representative snapshots corresponding to the different dipeptide conformers are shown superimposed on the graph. It is evident from the disconnectivity graph that in contrast to Ac-Ala-NH_2, the conformational space of Ac-Ser-NH_2 is quite rich.

lization, the C_5-I conformer is nearly degenerate with C_5-III. The free energy gap between the P_{II} and the C_7^{eq} conformers is somewhat higher than the value obtained for the Ac-Ala-NH_2 dipeptide, due to its enhanced enthalpic destabilization, as discussed earlier. The β_2 and α' conformers appear at the high free energy region of the *trans* funnel, and do not contribute substantially to the equilibrium thermodynamic properties at 298 K. This observation is consistent with the relative populations obtained for these conformers from our initial microsecond MD simulations (Supporting Information, Table S1). The C_7^{ax} conformer lies at the bottom of a competing funnel on the landscape, and is separated from the C_7^{eq} conformers by ≈ 7.8 kcal/mol. The α_D conformations lie on the top of the competing funnel, and from the organization of the FEL it is apparent that they would spontaneously relax to the C_7^{ax} basin. Similar to Ac-Ala-NH_2, the *cis* funnel for Ac-Ser-NH_2 consists of low-lying conformers, such as α_L and α_R, which do not have *trans* equivalents.

Emergent thermodynamic and kinetic properties: The heat capacity profiles of Ac-Ala-NH_2 and Ac-Ser-NH_2 provide further insight into how side-chain polarity modulates the emergent thermodynamic features of the landscape (Figure 4). For both the dipeptide sequences, there is a low temperature peak in the heat capacity profile, which results from the competition between the low-lying C_7^{eq} and C_5 conformers. Similar solid-solid transitions have been characterised in detail for atomic clusters,[111] where the interplay between enthalpy and entropy switches the free energy global minimum with temperature. The peak occurs at ≈ 150 K for Ac-Ala-NH_2, in excellent agreement with previous estimates from REMD and nested sampling simulations.[55] For Ac-Ser-NH_2, the peak is shifted to around 278 K, reflecting the relatively larger free energy gap between the C_7^{eq} and C_5 conformers.

In Figure 4, we show the free energy gap, ΔF, between the C_7^{eq} and the C_5 conformers as a function of temperature. At low temperatures (≤ 150 K), which closely mimic the conditions for creating the cooled jet in experiments, ΔF for the Ac-Ala-NH_2 dipeptide varies between 0.28 and 0.17 kcal/mol. These values result in a population ratio of 1.8 : 1 in favor of the C_7^{eq} conformer, in precise agreement with the predictions of Alonso and coworkers.[33] Under

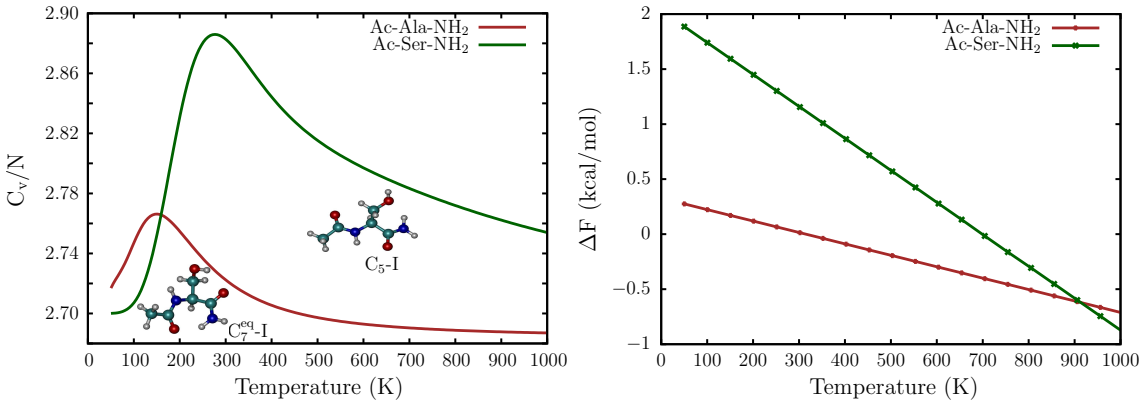

Figure 4. Left: The normalized heat capacity profile, C_v/N, computed from the database of minima for Ac-Ala-NH_2 and Ac-Ser-NH_2. Here, C_v is in reduced units of k_B, and scaled by the number of atoms, N. Right: The free energy gap, $\Delta F = F_{C_5} - F_{C_7{}^{eq}}$, between the C_7^{eq} and the C_5 conformers, as a function of temperature, for Ac-Ala-NH_2 and Ac-Ser-NH_2.

the same conditions, ΔF for Ac-Ser-NH_2 is between 1.9 and 1.6 kcal/mol, resulting in a population ratio of C_7^{eq} : $C_5 \geq 200 : 1$. These contrasting thermodynamic features of the FEL explain why Ac-Ala-NH_2 exists as mixture of C_7^{eq} and C_5 conformers in the gas phase, while Ac-Ser-NH_2 exists almost entirely in the C_7^{eq} rotameric state.

The rate constants as a function of temperature, corresponding to different conformational rearrangements of the dipeptides, are shown in Figure 5. As expected from the topography of the FELs, the C_5 to C_7^{eq} transition occurs on the fastest timescales at all temperatures. We estimate that this transition occurs approximately on the picosecond timescale for Ac-Ala-NH_2, while it is nearly two orders of magnitude slower in the case of Ac-Ser-NH_2. The C_7^{ax} to C_7^{eq} transition occurs approximately on the microsecond timescale. Transitions involving peptide bond isomerization, from *cis* to *trans* configurations are the slowest, with characteristic timescales of milliseconds or longer at low temperatures. In agreement with the findings of Garcia and coworkers,[108] we observe that temperatures greater than ≈ 350.0 K will be required to allow bond isomerizations on the sub-millisecond timescale. Both the $C_7^{ax} \rightarrow C_5$, and the *cis* $\rightarrow$ *trans* transition times seem to be unaffected by the presence of a polar side-chain in Ac-Ser-NH_2. Overall, we find that despite the inherent limitations of the harmonic superposition approach, and transition state theory, our estimated timescales

are in good agreement with those predicted by explicit dynamical simulations,[57] as well as DFT-based *ab initio* MD.[46]

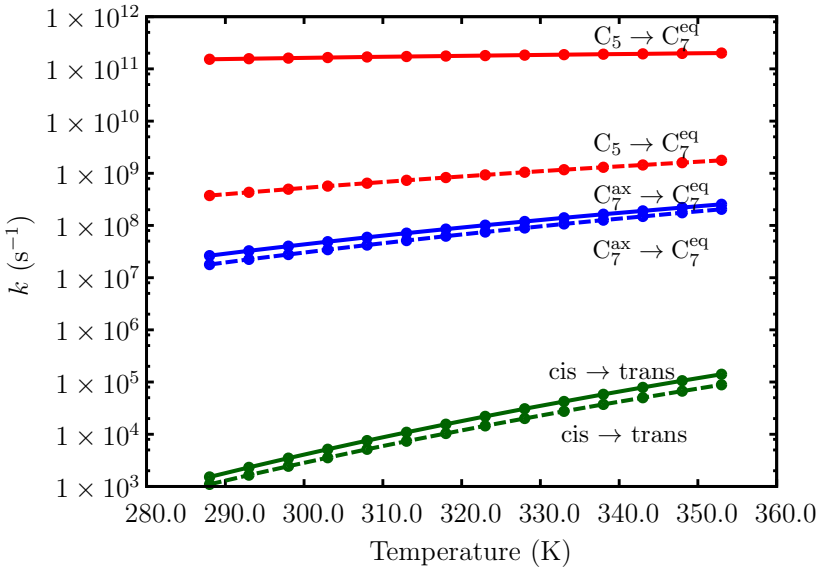

Figure 5. The rate constants as a function of temperature, estimated using the NGT method,[89,90] for different conformational transitions. Solid lines denote the values for Ac-Ala-NH_2, and the dashed lines denote the values for Ac-Ser-NH_2.

Reordering of minima upon reoptimization: All minima lying within the *trans* funnel of the two dipeptides were further reoptimized at the MP2 level using a 6-311++G(d,p) basis set. The normalized shifts in the ranking of minima, $\Delta R^{AMBER \rightarrow MP2}/N_{MIN}$ after reoptimization are illustrated in Figure 6. Here, a negative value denotes a shift towards a higher rank, indicating that a particular minimum is stabilized relative to other minima in the database, while a positive value of $\Delta R^{AMBER \rightarrow MP2}/N_{MIN}$ indicates destabilization with respect to other minima. For Ac-Ala-NH_2, the relative ordering of the various conformers in terms of potential energy is the same as the one obtained with AMBER. However, the P_{II} conformers are no longer characterized as minima on the MP2 surface, and they relax to the C_7^{eq} geometry. These 'new' C_7^{eq} minima (denoted as purple stars in Figure 6) are lower in energy than the C_5 minimum, and hence are assigned higher ranks.

The reorganization of the minima is more elaborate for Ac-Ser-NH_2. Although the C_7^{eq} and C_5 conformers still remain the lowest-energy conformers, we find that the α_D structures

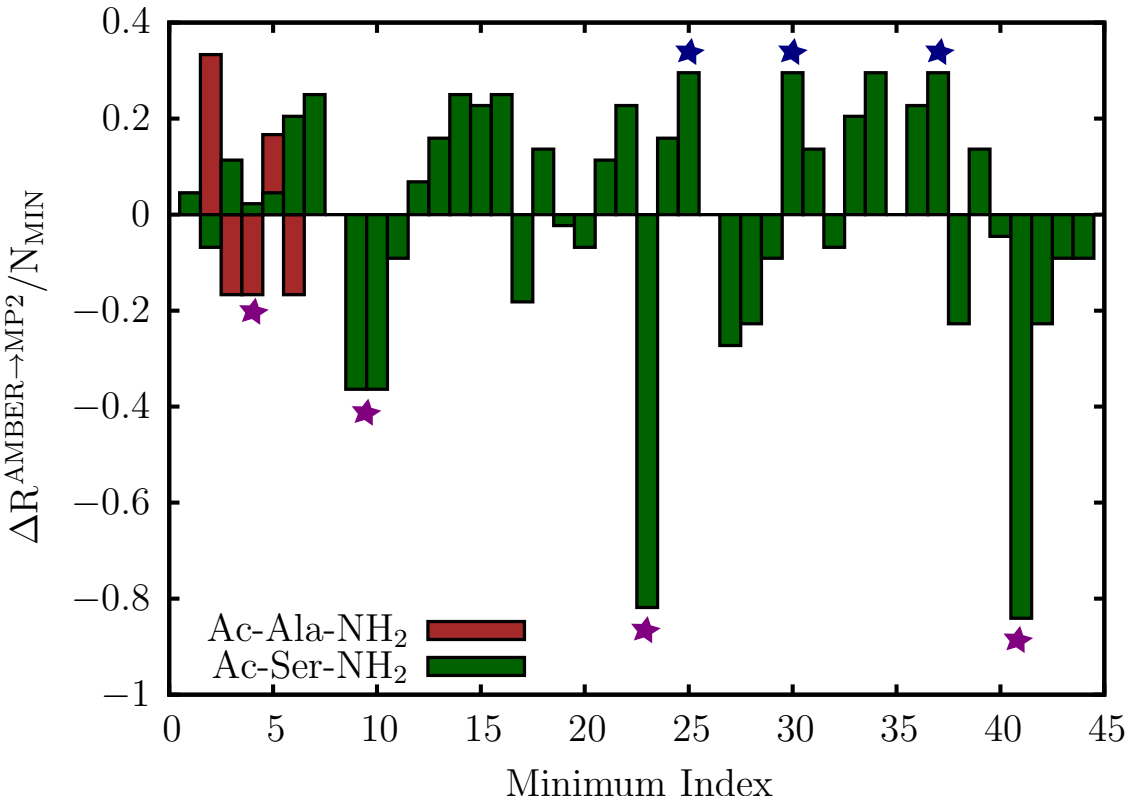

Figure 6. The normalized shift in ranking, $\Delta R^{\mathrm{AMBER}\rightarrow\mathrm{MP2}}/N_{\mathrm{MIN}}$, with respect to other minima after reoptimization at the MP2/6-311++G(d,p) level. Here, N_{MIN} denotes the total number of minima in the stationary point database. A positive value indicates a shift towards relatively lower ranks, as the structure is destabilized relative to other minima after reoptimization, while negative values indicate that the minima are relatively stabilized, and ranked more favourably after reoptimization. A purple star symbol is used to annotate those dipeptide conformations, which are maximally stabilized after reoptimization. The blue stars denote C_7^{ax} minima of Ac-Ser-NH$_2$, which are maximally destabilized after reoptimization at the MP2 level.

are more stabilized relative to the AMBER force field. In contrast, all the C_7^{ax} conformers are destabilized on the MP2 potential energy surface relative to other minima, and are associated with positive values of $\Delta R^{\mathrm{AMBER}\rightarrow MP2}/N_{\mathrm{MIN}}$ ranging from 0.22 and 0.29 (Figure 6).

On the MP2 potential energy surface, we find at least two α_D conformers (indices 27 and 42), which are lower in energy compared to C_7^{ax}. In fact, both these minima were originally in the C_{ax}^7 form on the AMBER landscape, and switched to α_D after reoptimization. In addition, two other C_7^{ax} conformers (indices 13 and 24) switch to the α_L geometry, through major changes in the ψ torsion, and are shifted to lower ranks. The α_L conformer does not appear as a true geometric minimum on the AMBER potential energy surface. This discrepancy suggests that despite the reasonable agreement with gas-phase experimental data, the AMBERff14SB force field has shortcomings, which need to be carefully evaluated in future studies. The most substantial shifts in ranking occur for two α' conformers (indices 23 and 41, denoted as purple stars in Figure 6) , which switch to the C_5 conformation after reoptimization. The other noticeable change in ranking occurs for minimum index 9 (denoted as a purple star in Figure 6), which was originally a P_{II} minimum on the AMBER surface, and switches to the C_5 geometry upon reoptimization at the MP2 level. In fact, similar to Ac-Ala-NH_2, the P_{II} conformers of Ac-Ser-NH_2 generally do not exist as potential energy minima on the MP2 surface, and switch to other forms, particularly C_5.

Rearrangement Pathways: The rearrangement pathways between the different conformers of Ac-Ala-NH_2, and Ac-Ser-NH_2, were computed using the AMBER force field, as well as electronic structure calculations at the MP2 level (Figures 7 and 8). To generate connected paths on the MP2 potential energy surface the transition states along a given rearrangement pathway (computed using the AMBER force field) were first reoptimized at the MP2/6-311++G(d,p) level. Next, the transition state geometry was perturbed in the directions parallel and antiparallel to the reaction coordinate (eigenvector associated with the imaginary frequency) to yield the adjoining minima. Using this protocol, we are able to exactly reproduce the relative potential energies, ΔV_{MP2} between the different minima reported in

the recent studies of Alonso and coworkers (Supporting Information, Table S2).[29,33]

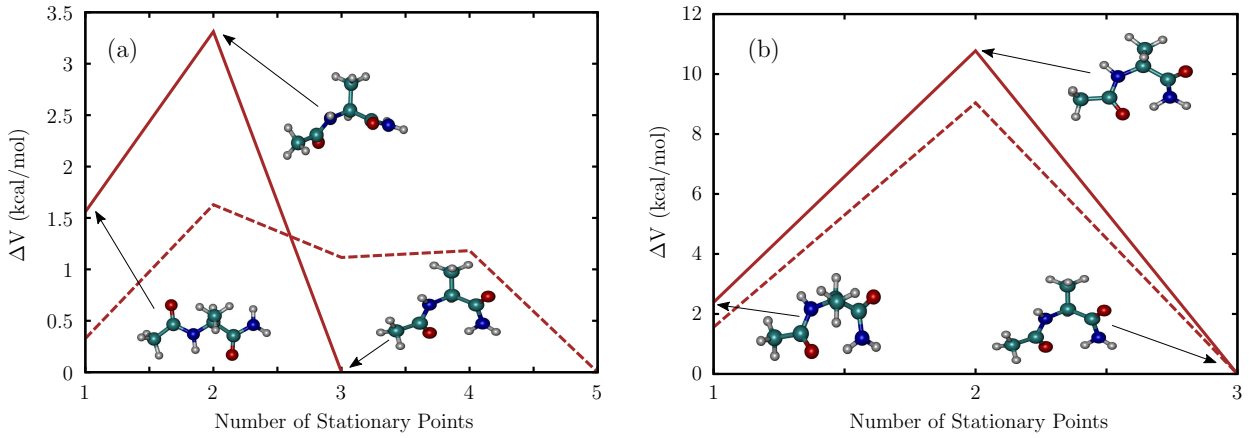

Figure 7. Transition paths between the different conformers of Ac-Ala-NH_2, computed using the AMBERff14SB force field (dashed lines), and at the MP2/6-311++G(d,p) level (solid lines). (a) C_5 to C_7^{eq} transition. (b) C_7^{ax} to C_7^{eq} transition. In these profiles, ΔV denotes the relative potential energy with respect to the global minimum.

The C_5 conformer of Ac-Ala-NH_2 switches to the C_7^{eq} structure via a P_{II}-type transition state (Figure 7). While the rearrangement occurs in a single step on the MP2 potential energy surface, it requires two steps on the AMBER landscape. The potential energy barrier, ΔV computed at the MP2 level (1.8 kcal/mol) is in excellent agreement with an early work by Schäfer and coworkers,[112] as well as more recent estimates from *ab initio* MD.[58] The corresponding barrier height estimated using the AMBER force field is around 1.3 kcal/mol.

The C_7^{ax} to C_7^{eq} rearrangement occurs in a single step. Although the transition state adopts a conformation similar to the C_7^{ax} form, its ϕ torsion angle switches from 60° to around 2°. A similar saddle point was identified along the minimum free energy path through the finite temperature string method, although the CHARMM22 force field was used to model the dipeptide.[57] The potential energy barrier, ΔV, for the transition is estimated to be around 7.5 kcal/mol with the AMBER force field, and about 8.4 kcal/mol at the MP2 level. These values are consistent with previous estimates from transition path sampling,[57,59,113] as well as milestoning.[114]

In Ac-Ser-NH_2, the transitions from the C_5-I and C_5-III forms to C_7^{eq}-I occur in two steps on the MP2 potential energy surface. On the other hand, the pathways computed using the

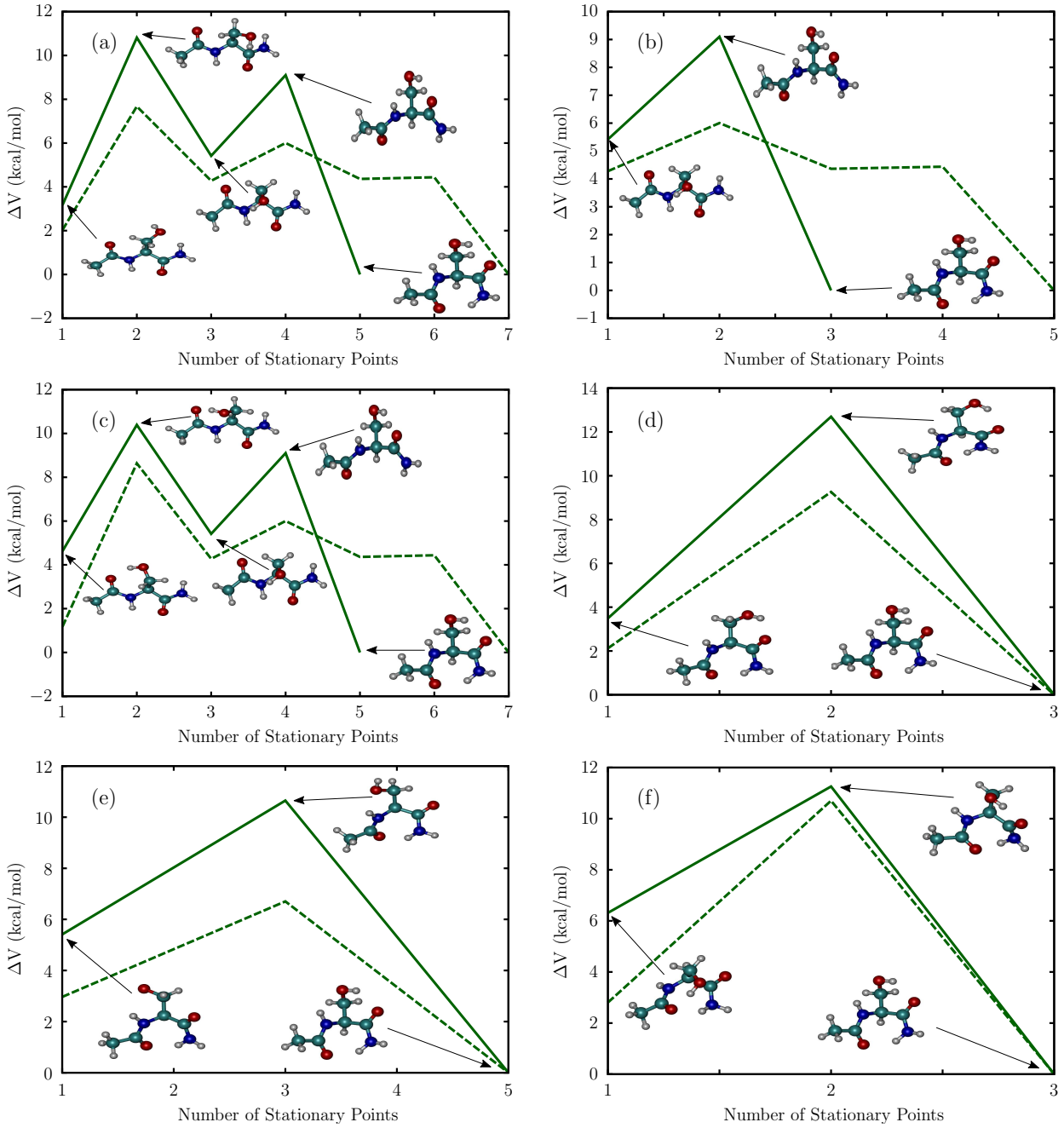

Figure 8. Transition paths between the different conformers of Ac-Ser-NH_2, computed using the AMBERff14SB force field (dashed lines), and at the MP2/6-311++G(d,p) level (solid lines). (a) C_5-I to C_7^{eq}-I (b)C_5-II to C_7^{eq}-I (c) C_5-III to C_7^{eq}-I (d) C_7^{eq}-II to C_7^{eq}-I (e) C_7^{eq}-III to C_7^{eq}-I (f) C_7^{ax} to C_7^{eq}-I. Similar to Figure 7, ΔV denotes the relative potential energy with respect to the global minimum.

AMBER force field consist of three intervening transition states (Figure 8 (a) and (c)). In contrast to the rearrangement mechanisms identified for Ac-Ala-NH_2, none of the $C_7^{eq} \rightarrow C_5$ pathways for this sequence proceed via a P_{II}-type transition state. Instead, the first step in both C_5-I $\rightarrow$ C_7^{eq}-I and C_5-III $\rightarrow$ C_7^{eq}-I transformations involves a conformational switch to the C_5-II minimum, through a transition state, in which the hydroxyl group of the Ser side-chain is approximately oriented between the equatorial and axial positions. The next step along the pathway on the MP2 surface involves a direct transformation to the C_7^{eq} form, through a C_7^{eq}-like transition state, having a relatively open structure (Figure 8). In the final step, seven-membered ring in C_7^{eq} forms in a completely downhill fashion. On the AMBER surface, there is an additional intervening step involving a rearrangement to a lower-energy C5-II structure, before the transition to the C_7^{eq} form can occur (Figures 8 (a), (b) and (c)).

The transformations between the different C_7^{eq} conformers occur in a single elementary step (Figure 8). The mechanism involves disruption and reformation of the hydrogen-bond between the amide hydrogen and the acetyl carbonyl oxygen, and concomitant rotation of the Ser side chain. The C_7^{eq}-II to C_7^{eq}-I rearrangement involves an abrupt change in the backbone configuration, as the ψ angle switches from around 50° in the C_7^{eq}-II minimum to approximately 2° in the transition state structure. For this step, we estimate a barrier height of $\approx$ 7.4 kcal/mol using AMBER, and 9.2 kcal/mol at the MP2 level. The C_7^{eq}-III $\rightarrow$ C_7^{eq}-I transition is not accompanied by such a substantial distortion of the protein backbone, and the ϕ angle changes by $\approx$ 17°. As a result, the corresponding barrier height,ΔV, for this transition is much less, and is estimated to be 3.7 kcal/mol using the AMBER force field, and around 5.2 kcal/mol at the MP2 level.

The C_7^{ax} to C_7^{eq}-I rearrangement in Ac-Ser-NH_2 proceeds via a α_L transition state. Both the ψ and ϕ torsions change substantially along the transition. This transition mechanism is significantly different from the one observed for Ac-Ala-NH_2, which proceeds through a C_7^{ax}-like transition state, and involves an abrupt change only in the ϕ torsion angle. Despite these different rearrangement mechanisms, the AMBER force field results in very similar barrier

heights (ΔV = 7.9 kcal/mol for Ac-Ser-NH_2, and 7.5 kcal/mol for Ac-Ala-NH_2) for the two dipeptides. This surprising equivalence rationalizes why we obtained very similar timescales for the $C_7^{ax} \rightarrow C_7^{eq}$ transitions at all temperatures (Figure 5). However, this equivalence of barrier heights is not supported by our MP2 calculations. ΔV corresponding to the $C_7^{ax} \rightarrow C_7^{eq}$ transition in Ac-Ser-NH_2 is predicted to be 4.9 kcal/mol, which is approximately half of the estimated MP2 barrier height for Ac-Ala-NH_2. This discrepancy may result from the relative destabilization of C_7^{ax} minima on the MP2 surface.

In contrast to earlier AMBER force fields,[115] the ff14SB variant also includes empirical corrections based on explicit solvent simulations of $(Ala)_5$,[63] and has been carefully fine-tuned to reproduce NMR data,[116,117] such as scalar J-couplings. The force field optimization with respect to solution-phase experiments could be one of the plausible reasons for the significant differences with respect to the gas-phase results obtained at the MP2 level of theory. Nonetheless, our results hint at possible deficiencies with the empirical force field, and emphasize the need for more careful benchmarking in future studies.

Conclusion

In a series of recent studies,[29,33] Alonso and coworkers demonstrated using Fourier transform microwave spectroscopy that the model peptide Ac-Ala-NH_2 exists as mixture of C_7^{eq} and C_5 conformers in the supersonic jet expansion, whereas the presence of polar side-chain in Ac-Ser-NH_2 conformationally locks the dipeptide in the C_7^{eq} conformation. We trace the origin of this behavior to the contrasting features of the underlying energy landscapes. At sufficiently low temperatures, which closely mimic the experimental conditions for creating a cooled jet, the free energy gap, ΔF, between the C_7^{ex} and C_5 conformers of Ac-Ala-NH_2 is around $k_B T$, suggesting that both conformers are present in the equilibrium distribution. In contrast, for Ac-Ser-NH_2, ΔF is at least $2k_B T$, and the C_7^{eq} conformer dominates the equilibrium population.

The presence of a polar side-chain results in distinct thermodynamic, as well as kinetic signatures. Although both dipeptides exhibit a low-temperature heat capacity peak, corresponding to the $C_7^{eq} \rightarrow C_5$ conformational switch, the transition occurs at a much lower temperature in Ac-Ala-NH_2. The rearrangements between the C_7^{eq} and C_5 forms also occurs at least an order of magnitude faster in Ac-Ala-NH_2. The interconversion between the C_7^{ax} and C_7^{eq} forms occurs on the microsecond timescale, and the dynamics seem to be independent of the sequence, despite obvious differences in the rearrangement mechanisms. However, refined calculations based on Moller-Plesset perturbation theory does suggest that the apparent free energy barrier for interconversion from the C_7^{ax} to the C_7^{eq} form could be lowered as a result of the systematic destabilization of nearly all C_7^{ax} minima on the MP2 surface.

There is some debate regarding the relevance of gas-phase studies on biomolecules, especially because water is ubiquitous within the cellular milieu. Besides acting as a lubricant, water molecules also significantly modulate the dynamics the protein folding via polarization fluctuations.[118] However, some recent reviews[119,120] on this subject show that much can be learnt regarding the fundamental stabilizing interactions in peptides from gas-phase studies. Inside cells, proteins/peptides may interact with different environments, such as membranes and hydrophobic pockets, and deciphering the gas-phase energy landscapes is critical for systematically comparing the perturbations induced by these surroundings. Many proteins even retain their native structures in solvent-free conditions, and in some cases the gas-phase structure could indeed be representative of the biologically active conformation.[121] As pointed out by Rossi and coworkers,[122] the gas-phase provides a "clean environment" for comparison between theory and experiment. Previous work on model dipeptides clearly suggest that an aqueous environment tends to 'flatten' the free energy surface,[35] and decrease the barriers between different conformations. Some low-lying gas-phase structures may be destabilized substantially, and structures with relatively open Ramachandran angles may be favored as a result of solvent-mediated interactions. Multiple studies based on both

ab initio[123] and molecular mechanics[97] methods predict that the C_7^{eq} conformation is not preferred in polar solvents, and the α_R conformation emerges as the new global minimum. In line with these previous studies, we anticipate that the relative ordering of the free energy minima for both Ac-Ala-NH_2 and Ac-Ser-NH_2 will change in the solution phase, although the global topographies of the landscapes are likely to be preserved.

Acknowledgement

D.J.W. gratefully acknowledges the EPSRC for financial support. D.C. is grateful to Prof. Dave Thirumalai for his mentorship, and for his inspiring thoughts on a diverse range of topics.

The authors declare no competing financial interest.

Supporting Information Available

Tabulated values of the number of snapshots corresponding to each conformer sampled along the MD trajectories; Figure illustrating the switch in geometry during local minimization; Snapshots corresponding to the low-lying C_7^{eq} and C_5 conformers of Ac-Ser-NH_2, with the hydrogen-bonding pattern explicitly shown; potential energy disconnectivity graphs. This material is available free of charge via the Internet at `http://pubs.acs.org/`.

References

(1) Dill, K. A.; MacCallum, J. L. The Protein-Folding Problem, 50 Years On. *Science* **2012**, *338*, 1042–1046.

(2) Dill, K. A.; Ozkan, S. B.; Shell, M. S.; Weikl, T. R. The Protein-Folding Problem. *Annu. Rev. Biophys.* **2008**, *37*, 289–316.

(3) Lindorff-Larsen, K.; Piana, S.; Dror, R. O.; Shaw, D. E. How Fast-Folding Proteins Fold. *Science* **2011**, *28*, 517–520.

(4) Senior, A. W.; Evans, R.; Jumper, J.; Kirkpatrick, J.; Sifre, L.; Green, T.; Qin, C.; Zidek, A.; Nelson, A. W. R.; Bridgland, A.; Penedones, H.; Peterson, S.; Simonyan, K.; Crossan, S.; Kohli, P.; Jones, D. T.; Silver, D.; Kavukcuoglu, K.; Hassabis, D. Improved protein structure prediction using potentials from deep learning. *Nature* **2020**, *577*, 706–710.

(5) Schuler, B.; Eaton, W. A. Protein folding studied by single-molecule FRET. *Curr. Opin. Struc. Biol.* **2008**, *18*, 16–26.

(6) Guinn, E. J.; Jagannathan, B.; Marqusee, S. Single-molecule chemo-mechanial unfolding reveals multiple transition state barriers in a small single-domain protein. *Nat. Commun.* **2015**, *6*, 6861.

(7) Onuchic, J. N.; ; Luthey-Schulten, Z.; Wolynes, P. G. Theory of Protein Folding: The Energy Landscape Perspective. **1997**, *48*, 545–600.

(8) Joseph, J. A.; Roder, K.; Chakraborty, D.; Mantell, R. G.; Wales, D. J. Exploring biomolecular energy landscapes. *Chem. Commun.* **2017**, *53*, 6974–6988.

(9) O'Brien, E. P.; Brooks, B.; Thirumalai, D. Effects of pH on proteins: Predictions for ensemble and single molecule pulling experiments. *J. Am. Chem. Soc.* **2012**, *134*, 979–987.

(10) Yang, A.-S.; Honig, B. On the pH Dependence of Protein Stability. *J. Mol. Biol.* **1993**, *231*, 459–474.

(11) Rami, B. R.; Udgaonkar, J. B. pH-Jump-Induced Folding and Unfolding Studies of Barstar: Evidence for Multiple Folding and Unfolding Pathways. *Biochemistry* **2001**, *40*, 15267–15279.

(12) Stagg, L.; Zhang, S.-Q.; Cheung, M. S.; Wittung-Stafshede, P. Molecular crowding enhances native structure and stability of α/β protein flavodoxin. *Proc. Natl. Acad. Sci. USA* **2007**, *104*, 18976–18981.

(13) Cheung, M. S.; Klimov, D.; Thirumalai, D. Molecular crowding enhances native state stability and refolding rates of globular proteins. *Proc. Natl. Acad. Sci. USA* **2005**, *102*, 4753–4758.

(14) Reddy, G.; Liu, Z.; Thirumalai, D. Denaturant-dependent folding of GFP. *Proc. Natl. Acad. Sci. USA* **2012**, *109*, 17832–17838.

(15) England, J. L.; Haran, G. Role of Solvation Effects in Protein Denaturation: From Thermodynamics to Single Molecules and Back. *Annu. Rev. Phys. Chem.* **2011**, *62*, 257–277.

(16) de Vries, M. S.; Hobza, P. Gas-phase Spectroscopy of Biomolecular Building Blocks. *Annu. Rev. Phys. Chem.* **2007**, *58*, 585–612.

(17) Biswal, H. S.; Loquais, Y.; Tardivel, B.; Gloaguen, E.; Mons, M. Isolated monohydrates of a model peptide chain: Effect of a first water molecule on the secondary structure of a capped phenylalanine. *J. Am. Chem. Soc.* **2011**, *133*, 3931–3942.

(18) Dian, B. C.; Longarte, A.; Zwier, T. S. Conformational dynamics in a dipeptide after single-mode vibrational excitation. *Science* **2002**, *296*, 2369–2373.

(19) Gloaguen, E.; De Courcy, B.; Piquemal, J. P.; Pilmé, J.; Parisel, O.; Pollet, R.; Biswal, H. S.; Piuzzi, F.; Tardivel, B.; Broquier, M.; Mons, M. Gas-phase folding of a two-residue model peptide Chain: On the importance of an interplay between experiment and theory. *J. Am. Chem. Soc.* **2010**, *132*, 11860–11863.

(20) Shubert, V. A.; Zwier, T. S. IR-IR-UV hole-burning: Conformation specific IR spectra in the face of UV spectral overlap. *J. Phys. Chem. A* **2007**, *111*, 13283–13286.

(21) Brenner, V.; Piuzzi, F.; Dimicoli, I.; Tardivel, B.; Mons, M. Spectroscopic evidence for the formation of helical structures in gas-phase short peptide chains. *J. Phys. Chem. A* **2007**, *111*, 7347–7354.

(22) James, W. H.; Baquero, E. E.; Shubert, V. A.; Choi, S. H.; Gellman, S. H.; Zwier, T. S. Single-conformation and diastereomer specific ultraviolet and infrared spectroscopy of model synthetic foldamers: α/β-peptides. *J. Am. Chem. Soc.* **2009**, *131*, 6574–6590.

(23) Gloaguen, E.; Tardivel, B.; Mons, M. Gas phase double-resonance IR/UV spectroscopy of an alanine dipeptide analogue using a non-covalently bound UV-tag: Observation of a folded peptide conformation in the Ac-Ala-NH2-toluene complex. *Struct. Chem.* **2016**, *27*, 225–230.

(24) Alonso, J. L.; Pérez, C.; Eugenia Sanz, M.; López, J. C.; Blanco, S. Seven conformers of L-threonine in the gas phase: A LA-MB-FTMW study. **2009**, *11*, 617–627.

(25) Sanz, M. E.; López, J. C.; Alonso, J. L. Six conformers of neutral aspartic acid identified in the gas phase. *Phys. Chem. Chem. Phys.* **2010**, *12*, 3573–3578.

(26) Lesarri, A.; Sánchez, R.; Cocinero, E. J.; López, J. C.; Alonso, J. L. Coded amino acids in gas phase: The shape of isoleucine. *J. Am. Chem. Soc.* **2005**, *127*, 12952–12956.

(27) Blanco, S.; Sanz, M. E.; López, J. C.; Alonso, J. L. Revealing the multiple structures of serine. *Proc. Natl. Acad. Sci. U. S. A.* **2007**, *104*, 20183–20188.

(28) Blanco, S.; Lesarri, A.; López, J. C.; Alonso, J. L. The gas-phase structure of alanine. *J. Am. Chem. Soc.* **2004**, *126*, 11675–11683.

(29) Cabezas, C.; Robben, M. A. T.; Rijs, A. M.; Pena, I.; Alonso, J. L. Fourier transform microwave spectroscopy of Ac-Ser-NH2: the role of side chain interactions in peptide folding. *Phys. Chem. Chem. Phys.* **2015**, *17*, 20274–20280.

(30) Leon, I.; Alonso, E. R.; Mata, S.; Cabezas, C.; Rodriguez, M. A.; Grabow, J. U.; Alonso, J. L. The role of amino acid side chains in stabilizing dipeptides: the laser ablation Fourier transform microwave spectrum of Ac-Val-NH2. *Phys. Chem. Chem. Phys.* **2017**, *19*, 24985–24990.

(31) Cabezas, C.; Varela, M.; Alonso, J. L. The Structure of the Elusive Simplest dipeptide Gly-Gly. *Angew. Chem.* **2017**, *129*, 6520–6525.

(32) Leon, I.; Alonso, E. R.; Mata, S.; Cabezas, C.; Alonso, J. L. Unveiling the Neutral Forms of Glutamine. *Angew. Chem.* **2019**, *58*, 16002–16007.

(33) Cabezas, C.; Varela, M.; Cortijo, V.; Jiminez, A. I.; Pena, I.; Daly, A. M.; Lopez, J. C.; Cativela, C.; Alonso, J. L. The alanine model dipeptide Ac-Ala-NH2 exists as a mixture of Ceq7 and C5 conformers. *Phys. Chem. Chem. Phys.* **2013**, *15*, 2580–2585.

(34) Leon, I.; Alonso, E. R.; Mata, S.; Alonso, J. L. A rotational study of the AlaAla dipeptide. *Phys.Chem.Chem.Phys.* **2020**, *22*, 13867.

(35) Tobias, D. J.; Brooks, C. L. Conformational equilibrium in the alanine dipeptide in the gas phase and aqueous solution: A comparison of theoretical results. *J. Phys. Chem.* **1992**, *96*, 3864–3870.

(36) Vymětal, J.; Vondrasek, J. The DF-LCCSD(T0) correction of the u/w force field dihedral parameters significantly influences the free energy profile of the alanine dipeptide. *Chem. Phys. Lett.* **2011**, *503*, 301–304.

(37) Grdadolnik, J.; Grdadolnik, S. G.; Avbelj, F. Determination of Conformational Preferences of Dipeptides Using Vibrational Spectroscopy. *J. Phys. Chem. B* **2008**, *112*, 2712–2718.

(38) Kaminsky, J.; Jensen, F. Force Field Modeling of Amino Acid Conformational Energies. *J. Chem. Theory Comput.* **2007**, *3*, 1774–1788.

(39) Head-Gordon, T.; Head-Gordon, M.; Frisch, M. J.; Brooks, C. L.; Pople, J. A. Theoretical Study of Blocked Glycine and Alanine Peptide Analogues. *J. Am. Chem. Soc.* **1991**, *113*, 5989–5997.

(40) Gould, I. R.; Cornell, W. D.; Hillier, I. H. A Quantum Mechanical Investigation of the Conformational Energetics of the Alanine and Glycine Dipeptides in the Gas Phase and in Aqueous Solution. *J. Am. Chem. Soc.* **1994**, *116*, 9250–9256.

(41) Vargas, R.; Garza, J.; Hay, B. P.; Dixon, D. A. Conformational Study of the Alanine Dipeptide at the MP2 and DFT Levels. *J. Phys. Chem. A* **2002**, *106*, 3213–3218.

(42) Improta, R.; Barone, V. Assesing the reliability of density functional methods in the conformational study of polypeptides: The treatment of intraresidue nonbonding interactions. *J. Comput. Chem.* **2004**, *25*, 1333–1341.

(43) Mackerell, A. D.; Feig, M.; Brooks, C. L. Extending the treatment of backbone energetics in protein force fields: Limitations of gas-phase quantum mechanics in reproducing protein conformational distributions in molecular dynamics simulation. *J. Comput. Chem.* **2004**, *25*, 1400–1415.

(44) Somani, S.; Wales, D. J. Energy landscapes and global thermodynamics for alanine peptides. *J. Chem. Phys.* **2013**, *139*, 121909.

(45) Mironov, V.; Alexeev, Y.; Mulligan, V. K.; Fedorov, D. G. A systematic study of minima in alanine dipeptide. *J. Comput. Chem.* **2019**, *40*, 297–309.

(46) Wei, D.; Guo, H.; Salahub, D. R. Conformational dynamics of an alanine dipeptide analog: An ab initio molecular dynamics study. *Phys. Rev. E.* **2001**, *64*, 011907.

(47) Wales, D. J. *Energy Landscapes*; Cambridge University Press, U.K., 2003.

(48) Wales, D. J. Energy landscapes: some new horizons. *Curr. Opin. Struct. Biol.* **2010**, *20*, 3–10.

(49) Wales, D. J.; Doye, J. P. K. Global Optimization by Basin-Hopping and the Lowest Energy Structures of Lennard-Jones clusters containing upto 110 Atoms. *J. Phys. Chem. A* **1997**, *101*, 5111–5116.

(50) Li, Z.; Scheraga, H. Monte Carlo-minimization approach to the multiple-minima problem in protein folding. *Proc. Natl. Acad. Sci. USA* **1987**, *84*, 6611–6615.

(51) Wales, D. J. Discrete Path Sampling. *Mol. Phys.* **2002**, *100*, 3285–3305.

(52) Wales, D. J. Some Further Applications of Discrete Path Sampling to Cluster Isomerization. *Mol. Phys.* **2004**, *102*, 891–908.

(53) Chekmarev, D. S.; Ishida, T.; Levy, R. M. Long-Time Conformational Transitions of Alanine Dipeptide in Aqueous Solution: Continuous and Discrete-State Kinetic Models. *J. Phys. Chem B* **2004**, *108*, 19487–19495.

(54) Ensing, B.; Vivo, M. D.; Liu, Z.; Moore, P.; Klein, M. L. Metadynamics as a Tool for Exploring Free Energy Landscapes of Chemical Reactions. *Acc. Chem. Res.* **2006**, *39*, 73–81.

(55) Burkoff, N. S.; Baldock, R. N. J.; Varnai, C.; Wild, D. L.; Csanyi, G. Exploiting molecular dynamics in Nested Sampling simulations of small peptides. *Comput. Phys. Commun.* **2016**, *201*, 8–18.

(56) Chen, M.; Cuendet, M. A.; Tuckerman, M. E. Heating and flooding: A unified approach for rapid generation of free energy surfaces. *J. Chem. Phys.* **2012**, *137*, 024102.

(57) Ren, W.; Vanden-Eijnden, E.; Maragakis, P.; Weinan, E. Transition pathways in complex systems: Application of the finite-temperature string method to the alanine dipeptide. *J. Chem. Phys.* **2005**, *123*, 134109.

(58) de Oliviera, C. A. F.; Hamelburg, D.; McCammon, J. A. Estimating kinetic rates from accelerated molecular dynamics simulations: Alanine dipeptide in explicit solvent as a case study. *J. Chem. Phys.* **2007**, *127*, 175105.

(59) Bolhuis, P. G.; Dellago, C.; Chandler, D. Reaction coordinates of biomolecular isomerization. *Proc. Natl. Acad. Sci. USA* **2000**, *97*, 5877–5882.

(60) Apostolakis, J.; Ferrara, P.; Calfisch, A. Calculation of conformational transitions and barriers in solvated systems: Application to the alanine dipeptide in water. *J. Chem. Phys.* **1999**, *110*, 2099–2108.

(61) Lavrich, R. J.; Plusquellic, D. F.; Suenram, R. D.; Fraser, G. T.; Hight Walker, A. R.; Tubergen, M. J. Experimental studies of peptide bonds: Identification of the C7eq conformation of the alanine dipeptide analog N-acetyl-alanine N-methylamide from torsion-rotation interactions. *J. Chem. Phys.* **2003**, *118*, 1253–1265.

(62) Case, D. A.; Darden, T. A.; Cheatham, T.; Simmerling, C. L.; Wang, J.; Duke, R. E.; Luo, R.; Walker, R. C.; Zhang, W.; Merz, K. M.; Roberts, B.; Hayik, S.; Roitberg, A.; Seabra, G.; Swails, J.; Goetz, A. W.; Kolossváry, I. AMBER 12. http://ambermd.org/, 2012.

(63) Maier, J. A.; Martinez, C.; Kasavajhala, K.; Wickstrom, L.; Hauser, K. E.; Simmerling, C. ff14SB: Improving the Accuracy of Protein Side Chain and Backbone Parameters from ff99SB. *J. Chem. Theory Comput.* **2015**, *11*, 3696–3713.

(64) Loncharich, R. J.; Brooks, B. R.; Pastor, R. W. Langevin dynamics of peptides: The frictional dependence of isomerization rates of N-actylananyl-N$'$-methylamide. *Biopolymers* **1992**, *32*, 523–535.

(65) Wales, D. J. GMIN: A program for finding global minima and calculating thermodynamic properties from basin-sampling. http://www-wales.ch.cam.ac.uk/software.html.

(66) Case, D. A.; Darden, T. A.; Cheatham, T.; Simmerling, C. L.; Wang, J.; Duke, R. E.; Luo, R.; Walker, R. C.; Zhang, W.; Merz, K. M.; Roberts, B.; Hayik, S.; Roitberg, A.; Seabra, G.; Swails, J.; Goetz, A. W.; Kolossváry, I. AMBER 9. http://ambermd.org/, 2006.

(67) Middleton, T. F.; Hernandez-Rojas, J.; Mortenson, P. N.; Wales, D. J. Crystals of Lennard-Jones solids. *Phys. Rev. B.* **2001**, *64*, 184201.

(68) Oakley, M. T.; Johnston, R. L. Exploring the Energy Landscapes of Cyclic Tetrapeptides with Discrete Path Sampling. *J. Chem. Theory Comput.* **2013**, *9*, 650–657.

(69) Chakraborty, D.; Sengupta, N.; Wales, D. J. Conformational Energy Landscape of the Ritonavir Molecule. *J. Phys. Chem. B* **2016**, *120*, 4331–4340.

(70) Liu, D.; Nocedal, J. On the Limited Memory Method for Large Scale Optimization. *Math. Program.* **1989**, *45*, 503–528.

(71) Carr, J. M.; Wales, D. J. Folding Pathways and Rates for the Three-Stranded beta-sheet Peptide Beta3s Using Discrete Path Sampling. *J. Phys. Chem. B* **2008**, *112*, 8760–8769.

(72) Farrell, J. D.; Lines, C.; Shepherd, J. J.; Chakrabarti, D.; Miller, M. A.; Wales, D. J. Energy landscapes, structural topologies and rearrangement mechanisms in clusters of dipolar particles. *Soft Matter* **2013**, *9*, 5407–5416.

(73) Evans, D. E.; Wales, D. J. Folding of the GB1 Hairpin Peptide from Discrete Path Sampling. *J. Chem. Phys.* **2004**, *121*, 1080–1090.

(74) Chakraborty, D.; Collepardo-Guevara, R.; Wales, D. J. Energy Landscapes, Folding

Mechanism, and Kinetics of RNA Tetraloop Hairpins. *J. Am. Chem. Soc.* **2014**, *136*, 18052–18061.

(75) Chakraborty, D.; Chebaro, Y.; Wales, D. J. A multifunnel energy landscape encodes the competing α-helix and β-hairpin conformations for a designed peptide. *Phys. Chem. Chem. Phys.* **2020**, *22*, 1359–1370.

(76) Chakraborty, D.; Wales, D. J. Energy Landscape and Pathways for Transitions between Watson-Crick and Hoogsteen Base Pairing in DNA. *J. Phys. Chem. Lett.* **2018**, *9*, 229–241.

(77) Chakraborty, D.; Wales, D. J. Dynamics of an adenine-adenine RNA conformational switch from discrete path sampling. *J. Chem. Phys.* **2019**, *150*, 125101.

(78) Murrell, J. N.; Laidler, K. J. Symmetries of activated complexes. *Trans. Faraday Soc.* **1968**, *64*, 371–377.

(79) Trygubenko, S. A.; Wales, D. J. A Doubly Nudged Elastic Band Method for Finding Transition States. *J. Chem. Phys.* **2004**, *120*, 2082–2094.

(80) Henkelman, G.; Jònsson, H. A dimer method for finding saddle points on high dimensional potential surfaces using only first derivatives. *J. Chem. Phys.* **1999**, *111*, 7010–7022.

(81) Henkelman, G.; Uberuaga, B. P.; Jònsson, H. A climbing image nudged elastic band method for finding saddle points and minimum energy paths. *J. Chem. Phys.* **2000**, *113*, 9901–9904.

(82) Munro, L. J.; Wales, D. J. Defect Migration in Crystalline Silicon. *Phys. Rev. B.* **1999**, *59*, 3969–3980.

(83) Wales, D. J. OPTIM: A program for optimising geometries and calculating pathways. http://www-wales.ch.cam.ac.uk/software.html.

(84) Wales, D. J. PATHSAMPLE: A program for generating connected stationary point databases and extracting global kinetics. http://www-wales.ch.cam.ac.uk/software.html.

(85) Strodel, B.; Whittleston, C. W.; Wales, D. J. Thermodynamics and Kinetics of Aggregation for the GNNQQNY Peptide. *J. Am. Chem. Soc.* **2007**, *129*, 16005–16014.

(86) Dijkstra, E. W. A Note on Two Problems in Connexion with Graphs. *Numer. Math.* **1959**, *1*, 269–271.

(87) Hoare, M. R.; McInnes, J. J. Statistical mechanics and morphology of very small atomic clusters. *Faraday Discuss. Chem. Soc.* **1976**, *61*, 12–24.

(88) Hoare, M. R. *Advances in Chemical Physics*; John Wiley and Sons, USA, 1979; Vol. 40; pp 49–129.

(89) Stevenson, J. D.; Wales, D. J. *J. Chem. Phys.* **2014**, *141*, 041104.

(90) Wales, D. J. Calculating Rate Constants and Committor Probabilities for Transition Networks by Graph Transformation. *J. Chem. Phys.* **2009**, *130*, 204111(1)–204111(7).

(91) Becker, O. M.; Karplus, M. The topology of multidimensional potential energy surfaces: theory and application to peptide structure and kinetics. *J. Chem. Phys.* **1997**, *106*, 1495–1517.

(92) Wales, D. J.; Miller, M. A.; Walsh, T. R. Archetypal Energy Landscapes. *Nature* **1998**, *394*, 758–760.

(93) Krivov, S. V.; Karplus, M. Hidden complexity of free energy surfaces for peptide (protein) folding. *Proc. Natl. Acad. Sci. USA* **2004**, *101*, 14766–14770.

(94) Wales, D. J. Perspective: Insight into reaction coordinates and dynamics from the potential energy landscape. *J. Chem. Phys.* **2015**, *142*, 130901.

(95) Cabezas, C.; Varela, M.; Alonso, J. L. Probing the γ-Turn in a Short Proline Dipeptide Chain. *ChemPhysChem* **2013**, *14*, 2539–2543.

(96) Frisch, M. J. et al. Gaussian09 Revision E.01. Gaussian Inc. Wallingford CT 2009.

(97) Rubio-Martinez, J.; Tomas, M. S.; Perez, J. J. Effect of the solvent on the conformational behavior of the alanine dipeptide deduced from MD simulations. *J. Mol. Graph. Model.* **2017**, *78*, 118–128.

(98) Strodel, B.; Wales, D. J. Free energy surfaces from an extended harmonic superposition approachand kinetics for alanine dipeptide. *Chem. Phys. Lett.* **2008**, *466*, 105–115.

(99) Beachy, M. D.; Chasman, D.; Murphy, R. B.; Halgren, T. A.; Friesner, R. A. Accurate ab Initio Quantum Chemical Determination of the Relative Energetics of Peptide Conformations and Assessment of Empirical Force Fields. *J. Am. Chem. Soc.* **1997**, *119*, 5908–5920.

(100) Bohm, H.-J.; Brode, S. Ab Initio SCF Calculations on Low-Energy Conformers of V-Acetyl-TV'-methylalaninamide and iV-Acetyl-A'-methylglycinamide. *J. Am. Chem. Soc.* **1991**, *113*, 7129–7135.

(101) Hornak, V.; Abel, R.; Okur, A.; Strockbine, B.; Roitberg, A.; Simmerling, C. Comparison of multiple AMBER force fields and development of improved protein backbone parameters. *Proteins* **2006**, *65*, 712–725.

(102) Grubisic, S.; Brancato, G.; Barone, V. An improved AMBER force field for a,a-dialkylated peptides: intrinsic and solvent-induced conformational preferences of model systems. *Phys. Chem. Chem. Phys.* **2013**, *15*, 17395–17407.

(103) de M. Seabra, G.; Walker, R. C.; Elstner, M.; Case, D. A.; Roitberg, A. Implementation of the SCC-DFTB Method for Hybrid QM/MM Simulations within the Amber Molecular Dynamics Package. *J. Phys. Chem. A* **2007**, *111*, 5655–5664.

(104) Perczel, A.; Farkas, O.; Jakli, I.; Topol, I. A.; Csizmadia, I. G. Peptide Models. XXXIII. Extrapolation of Low-LevelHartreeFock Data of Peptide Conformation to LargeBasis Set SCF, MP2, DFT, and CCSD(T) Results. TheRamachandran Surface of Alanine Dipeptide Computedat Various Levels of Theory. *J. Comput. Chem.* **2003**, *24*, 1026–1042.

(105) Phillip, D. M.; Friesner, R. A. MixedAb InitioQMrMM Modeling UsingFrozen Orbitals and Tests with AlanineDipeptide and Tetrapeptide. *J. Comput. Chem.* **1998**, *20*, 1468–1494.

(106) Grenie, Y.; Avignon, M.; Garrigou-Lagrange, C. Molecular Structure Study of Dipeptides Isolated in an Argon matrix by Infrared Spectropscopy. *J. Mol. Struc.* **1975**, *24*, 293–307.

(107) Scherer, G.; Kramer, M. L.; Schutkowski, M.; Reimer, U.; Fischer, G. Barriers to rotation of secondary amide peptide bonds. *J. Am. Chem. Soc.* **1998**, *120*, 5568–5574.

(108) Neale, C.; Pomes, R.; Garcia, A. E. Peptide Bond Isomerization in High-Temperature Simulations. *J. Chem. Theory Comput.* **2016**, *12*, 1989–1999.

(109) Doshi, U.; Hamelberg, D. Reoptimization of the AMBER Force Field Parameters for Peptide Bond (Omega) Torsions Using Accelerated Molecular Dynamics. *J. Phys. Chem. B* **2008**, *113*, 16590–16595.

(110) Mirijaninan, D. T.; Mannige, R. V.; Zuckermann, R. N.; Whitelam, S. Development and use of an atomistic CHARMMbased forcefield for peptoid simulation. *J. Comput. Chem.* **2014**, *35*, 360–370.

(111) Doye, J. P. K.; Miller, M. A.; Wales, D. J. The double-funnel energy landscape of the 38-atom Lennard-Jones cluster. *J. Chem. Phys.* **1999**, *110*, 6896–6906.

(112) Frey, R. F.; Coffin, J.; Newton, S. Q.; Ramek, M.; Cheng, V. K. W.; Momany, F. A.; Schäfer, L. Importance of Correlation-Gradient Geometry Optimization for Molecular Conformational Analyses. *J. Am. Chem. Soc.* **1992**, *114*, 5369–5377.

(113) Zhou, H.; Tao, P. Dynamics Sampling in Transition Pathway Space. *J. Chem. Theory Comput.* **2018**, *14*, 14–29.

(114) Wei, W.; Elber, R. ScMile: A Script to Investigate Kinetics with Short Time Molecular Dynamics Trajectories and the Milestoning Theory. *J. Chem. Theory Comput.* **2020**, *16*, 860–874.

(115) Cornell, W. D.; Cieplak, P.; Bayly, C. I.; Gould, I. R.; Merz, K. M.; Ferguson, D. M.; Spellmeyer, D. C.; Fox, T.; Caldwell, J. W.; Kollman, P. A. A Second Generation Force Field for the Simulation of Proteins, Nucleic Acids, and Organic Molecules. *J. Am. Chem. Soc.* **1995**, *117*, 5179–5197.

(116) Best, R. B.; Buchete, N. V.; Hummer, G. Are Current Molecular Dynamics Force Fields too Helical? *Biophys. J.* **2008**, *95*, L07–L09.

(117) Graf, J.; Nguyen, P. H.; Stock, G.; Schwalbe, H. Structure and Dynamics of the Homologous Series of Alanine Peptides: A Joint Molecular Dynamics/NMR Study. *J. Am. Chem. Soc.* **2007**, *129*, 1179–1189.

(118) Mukherjee, S.; Mondal, S.; Bagchi, B. Mechanism of Solvent Control of Protein Dynamics. *Phys. Rev. Lett.* **2019**, *122*, 058101.

(119) Meyer, T.; Gabelica, V.; Grubmüller, H.; Orozco, M. Proteins in the gas phase. *WIREs Comput. Mol. Sci.* **2013**, *3*, 408–425.

(120) Marcoux, J.; Robinson, C. V. Twenty Years of Gas Phase Structural Biology. *Structure* **2013**, *21*, 1541–1550.

(121) Pereverzev, A.; Boyarkin, O. V. Exploring the relevance of gas-phase structures to biology: cold ion spectroscopy of the decapeptide neurokinin A. *Phys. Chem. Chem. Phys.* **2017**, *19*, 3468–3472.

(122) Baldauf, C.; Rossi, M. Going clean: structure and dynamics of peptides in the gas phase and paths to solvation. *J. Phys.: Condens. Matt.* **2015**, *27*, 493002.

(123) Wang, Z.-X.; Duan, Y. Solvation Effects on Alanine Dipeptide: AMP2/cc-pVTZ//MP2/6-31G** Study of (ϕ,ψ) Energy Maps and Conformers in the Gas Phase, Ether, and Water. *J. Comput. Chem.* **2004**, *25*, 1699–1716.

Graphical TOC Entry